

Article

Copper Metallopolymer Catalyst for the Electrocatalytic Hydrogen Evolution Reaction (HER)

Sait Elmas ^{1,*}, Thomas J. Macdonald ², William Skinner ³, Mats Andersson ^{1,*} and Thomas Nann ⁴¹ Institute for NanoScale Science & Technology, Flinders University, Bedford Park, SA 5042, Australia² Department of Chemistry, University College London, London WC1H 0AJ, UK; tom.macdonald@ucl.ac.uk³ Future Industries Institute, University of South Australia Mawson Lakes Campus, Mawson Lakes, SA 595, Australia; william.skinner@unisa.edu.au⁴ School of Mathematical and Physical Sciences, University of Newcastle, Callaghan, NSW 2308, Australia; thomas.nann@newcastle.edu.au

* Correspondence: sait.elmas@flinders.edu.au (S.E.); mats.andersson@flinders.edu.au (M.A.);

Tel.: +61-8820-12684 (S.E.)

Received: 14 November 2018; Accepted: 5 January 2019; Published: 10 January 2019



Abstract: Conjugated polymers with stabilizing coordination units for single-site catalytic centers are excellent candidates to minimize the use of expensive noble metal electrode materials. In this study, conjugated metallopolymer, P_{OS}[Cu], was synthesized and fully characterized by means of spectroscopical, electrochemical, and photophysical methods. The copper metallopolymer was found to be highly active for the electrocatalytic hydrogen generation (HER) in an aqueous solution at pH 7.4 and overpotentials at 300 mV vs. reversible hydrogen electrode (RHE). Compared to the platinum electrode, the obtained overpotential is only 100 mV higher. The photoelectrochemical tests revealed that the complexation of the conjugated polymer P_{OS} turned its intrinsically electron-accepting (p-type) properties into an electron-donor (n-type) with photocurrent responses ten times higher than the organic photoelectrode.

Keywords: copper; metallopolymer; photocurrent; electrocatalysts; hydrogen evolution reaction; p- and n-type photoresponse

1. Introduction

Conducting and/or conjugated polymers (CPs) are promising materials for organic photovoltaics [1–5]. Beyond their potential use in photovoltaics, CPs are already successfully implemented in many other commercialized electronic devices [6]. Due to their conductive nature, intrinsic semi-conducting properties and the precious advantages of “cheap plastics”, CPs are considered as one of the emerging material classes with much potential, which is not fully explored yet. Especially in the field of metallopolymer or metallosupramolecular polymers, where conducting polymers are complexed with single-site metal centers, there is a lack of research to tap into applications, where the use of metals is indispensable [7]. Organic–inorganic hybrid materials, with new optoelectronic properties, pave the way for potential applications, such as electro and photo catalysts as well as photo electrode materials with improved electronic and optical behaviors [8]. Single-site catalysts in metallopolymers as an alternative to nanoparticulate noble metals can be exposed for photo/-electrocatalysis to make every atom count [9]. Among the conductive/conjugated polymers, the poly(heteroarylene) methines (PHAMs) are well suited to host a series of transition metals into the conjugated polymer backbone. Further to this, their ease of synthesis and structural modification makes them attractive to synthesize metallopolymers for applications of choice. Even though a series

of PHAMs polymers are already reported in the literature, their potential applications were mostly limited to photovoltaics, optical devices, and close research fields.

Since the preliminary works of Jenekhe et al. [10] on the polymer class of poly(heteroarylene) methines (PHAMs) in 1986, there has been significant progress on the synthesis and modification of so-called “low-bandgap polymers”. Their peculiar low band-gap [11] makes them highly interesting as materials for organic photovoltaics (OPV) [3] and non-linear applications in photonics [12,13] because they absorb light in the visible range of the spectral light. Their applications in ordered ultrathin films with well-defined architecture using the Langmuir–Blodgett (LB) technique [14] or as sensing material for DNA [15] were also reported. Since PHAMs are known to show tuneable optoelectronic properties, so far most research activities have focused on the substitution effects on pendant heteroaryl units, the aromatic backbone [16,17], and the methylene bridges [18] where immediate influences on the band-gap positions and the band-gap sizes are achieved. Further modifications are known wherein the ratio between aromatic and quinonoidal systems influences the conductivity of the polymeric materials [19,20]. As a consequence of further tailoring of the optoelectronic properties, building blocks with specific properties were incorporated into the poly(heteroarylene) methine backbone, where multistep organic synthesis is involved [21]. Other than that, there is nothing much reported on PHAMs polymers and their metallopolymer at all.

We have synthesized a new polymer based on the PHAMs structure and complexed the polymer with copper. Herein, in opposition to the polymer structures known in the literature, the phenoxy functional groups were introduced into the ortho position of the pendant aromatic moieties. Besides the changes in the electronic structure of the polymer itself, the position of the phenoxy group made it possible to introduce transition metals into the repetitive chelating units (Figure 1). The combination of the hard (oxygen) and soft (sulfur) donors that cover the units allows a wide range of transition metals for complexation. Using copper (Cu), the metallopolymer revealed activities for the electrocatalytic hydrogen evolution reaction (HER) at overpotentials comparable to a platinum electrode in a phosphate buffered buffer saline solution (PBS) and at neutral pH 7.4. However, in opposition to the previously reported Cu metallopolymer (Cu MP) with a redox-active hydroquinone/benzoquinone pendant unit [22], the current Cu MP did not show any significant activity towards the oxygen reduction reaction (ORR). To the best of our knowledge, this is the first Cu PHAM electrode material showing activities toward HER at overpotentials close to a Pt electrode and at neutral pH. In addition to the HER activities, the organic/inorganic hybrid material showed an increase of photocurrent and a switch from a p-type (organic) to n-type (hybrid) photo-response under 1.5 air mass (1.5 AM) artificial sunlight, which has not been reported so far.

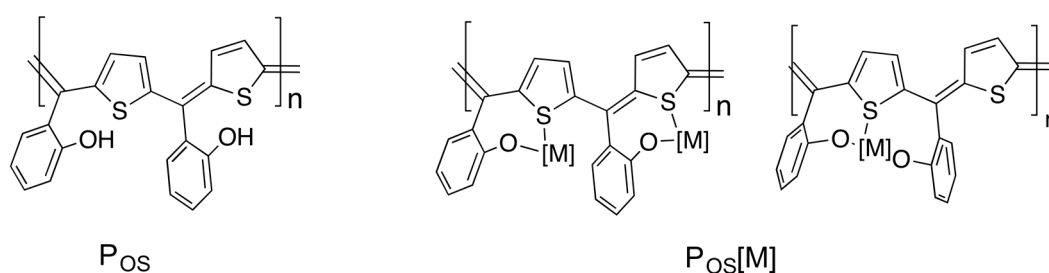


Figure 1. Chemical structures of the poly(heteroarylene) methine polymer P_{OS} and its metal complex $P_{OS}[M]$, where the indices OS represent bi- or tridentate coordinating modes and [M] is a metal center with any co-ligands.

2. Materials and Methods

1,4-dioxane (Emsure, Darmstadt, Germany 99.5%), thiophene (Aldrich, St. Louis, MO, USA, $\geq 99\%$), salicylaldehyde (Aldrich, 98%), sulfuric acid (Scharlau, Barcelona, Spain, 95–97%), and copper(II) acetate monohydrate (Aldrich) were obtained without further purification. All reactions were performed under ambient conditions at elevated temperatures.

UV/Vis spectra of the polymer and the copper-metallopolymers were recorded on a Varian UV/Vis spectrometer in acetonitrile using a quartz cuvette with an optical path length of 1.0 cm.

X-ray photoelectron spectroscopy (XPS) was performed with a Kratos Ultra DLD spectrometer, using monochromatic Al $k\alpha$ radiation ($h\nu = 1486.7$ eV). The system is equipped with a magnetically confined charge compensation system (low energy electrons are confined and transported to the sample surface by a magnetic field). Spectra were recorded using an acceleration voltage of 15 keV at a power of 225 W. Survey spectra were collected with a pass energy of 160 eV and an analysis area of $300 \mu\text{m} \times 700 \mu\text{m}$. Data analysis was performed with CasaXPS software (Casa Software Ltd.) and selected graphs were plotted with the Qti Plot software.

Cyclic voltammograms were recorded in a three-electrode configured electrochemical cell on an AUTOLAB potentiostat. A platinum rod was used as a counter electrode (CE) and the deposited films on gold substrates acted as working electrodes (WE). All recorded currents are referred to as Ag|AgCl (3 M). For the fabrication of the working electrodes gold substrates (100 nm Au with 40 nm Ti sublayer on microscope slides, obtained from RDLI Inc.) were coated with the polymer P_{OS} and $P_{OS}[Cu]$ respectively. Hydrogen evolution reactions (HER) were recorded on an AUTOLAB potentiostat using potentiostatic cyclic voltammetry methods. Here, the materials P_{OS} and $P_{OS}[Cu]$ were drop-casted on a gold substrate with $1 \times 1 \text{ cm}^2$ surface area acted as the working electrode (WE), each. A platinum rod was used as a counter electrode (CE) and Ag|AgCl (3 M KCl) acted as reference electrode (RE). The cyclic voltammograms (CV) were recorded at 100 mV/s in the potential range of 0.2 to -1 volts vs. Ag|AgCl (3 M KCl). For better comparisons, the recorded working potentials vs. Ag|AgCl (3 M KCl) were converted into the reversible hydrogen electrode (RHE) according to the equation $E_{(RHE)} = E_{(Ag|AgCl)} + 0.059 \cdot \text{pH} + 0.210 \text{ V}$, where pH of 0.1 M PSS was 7.4.

Hydrogen was measured by gas chromatography using a Hewlett Packard 5890 series II GC with a thermal conductivity detector (TCD) and employing a molecular sieve 5 A (80–100 mesh) 2 m column run at 60°C with argon as the carrier gas.

2.1. Synthesis of P_{OS} and $P_{OS}[Cu]$

Poly(thiophene-2,5-diyl)(o-hydroxybenzylidene), P_{OS} : Thiophene (2 mL, 2.1 g, 25 mmol), o-hydroxybenzaldehyde (2.96 mL, 3.39 g, 27.75 mmol) and 0.5 mL sulphuric acid (97%) were dissolved in 10 mL 1,4-dioxane and refluxed for 20 h at 80°C . The formed black polymer was precipitated by adding 20 mL methanol/water mixture (1/1) and washed twice with cold methanol/water (1/1). The black solid was then re-dissolved in THF and transferred into a round-bottom flask. After removal of all solvents and volatiles on the rotary evaporator, the polymer was obtained as black, crystalline powder (3.5 g).

Polymer complex with Cu(II) acetate, $P_{OS}[Cu]$: The polymer P_{OS} (1 g, 5.33 mmol referred to the MW of one repetition unit) and copper(II) acetate monohydrate (1 g, 5.01 mmol) were dispersed in 20 mL MeOH and refluxed for 24 h at 60°C . After removal of all volatiles and solvents on the rotary evaporator, the brown fine powder was washed 3 times with THF and dried in vacuum. The copper metallopolymers were obtained almost quantitatively as a brown fine powder, which is sparingly to non-soluble in most common organic solvents.

2.2. Electrode Preparation

Polymer $P_{OS}[Cu]$ spin-coat deposition: P_{OS} films were prepared using a Laurell WS-650S-6NPP/LITE spin coater (North Wales, PA, USA). The spin-coating solution consisted of 5 mL terpineol, 200 mg of the metallopolymers, and 5 drops acetylacetone. The $P_{OS}[Cu]$ was spin-coated onto a gold surface at 500 RPM for 10 s, followed by ramping to 2000 RPM for 30 s. These parameters resulted in a uniform coating of $P_{OS}[Cu]$ across the gold surface. Terpineol was then evaporated using an O_2 furnace at 250°C for 30 min. The heating rate was set to $5^\circ\text{C}/\text{min}$. The P_{OS} film thickness was confirmed to be $\sim 100 \mu\text{m}$ using a profilometer (Bruker, Billerica, MA, USA, Dektak XT). The spin-coated $P_{OS}[Cu]$

was mounted into the photoelectrochemical (PEC) for the chronoamperometric tests under 1.5 AM artificial sunlight.

Drop-casting of P_{OS} and $P_{OS}[Cu]$ for electrocatalytic tests (HER): P_{OS} and $P_{OS}[Cu]$ (10 mg) were dispersed in 20 mL iso-propanol (iPrOH) and sonicated for 30 min in an ultrasonic bath (Fisher Scientific FB15047), each. The dispersion was then slowly dropped onto the surface of gold substrates and the substrates were heated from the rear side with a heating gun until a clear black film was formed on the surface. The substrates were held with tweezers at a distance of 15–20 cm from the heating gun to avoid overheating of the films. The temperature of the heating gun was set to 150 °C. To obtain reasonable films the dropping sequence was adjusted to the complete evaporation of previous droplets. Occasionally the substrates were slightly tilted up and down to focus the evaporating droplets to vacant surface areas. The resulting polymer and metallopolymer electrodes were then air-dried and the active surface area was limited to $1.5 \times 1.5 \text{ cm}^2$ covered with film by wiping off the excess of film with KimTech Wipes moistened with iPrOH. The prepared electrodes were then mounted immediately into the electro-chemical cell for electrocatalytic HER tests.

3. Results and Discussion

3.1. Synthesis and Characterization of P_{OS} and $P_{OS}[Cu]$

For the synthesis of the polymer P_{OS} , we followed the protocol reported by Jenekhe [19,23]. Typically, thiophene, the aromatic aldehyde, and catalytic amounts of sulfuric acid were added in a one-pot-reaction and the mixture was refluxed overnight. After removing the solvents and the volatiles the polymer was obtained as black chunky solid and analyzed by UV/Vis, cyclic voltammetry (CV), and XPS. The polymer was slightly soluble in common organic solvents allowing purification by washing out unreacted starting materials and oligomer residuals. The best solubility was observed in dimethyl sulfoxide (DMSO) or acetonitrile (AN). The Cu metallopolymer was obtained as a dark brown, fine powder. As a consequence of the higher molecular weight, the metallopolymer became comparably poorly soluble in organic solvents indicating successful complexation.

The UV/Vis absorption spectra of the polymer P_{OS} and its complex compound with Cu(II) were recorded in AN. For comparisons, the Cu(II) acetate precursor was recorded in the same solvent. As depicted in Figure 2a the polymer P_{OS} shows five distinct absorption peaks (A 250 nm, B 276/286 nm, C 317 nm, D 393 nm, E 470/504, where two of them are in the range of the visible light. Among them, the absorption bands B and E appear with a shoulder, each.

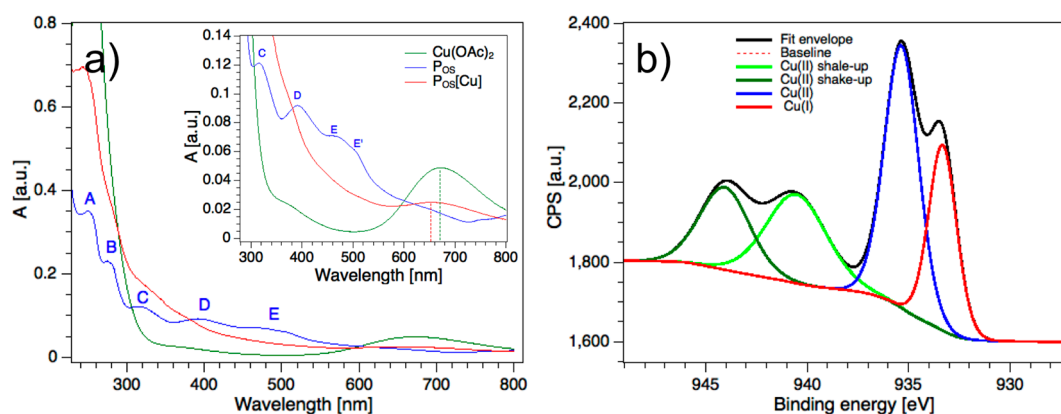


Figure 2. (a) UV/Vis absorption spectra of the polymer P_{OS} and its coordination compound $P_{OS}[Cu]$ (inset) in acetonitrile; (b) binding energies of the Cu 2p core levels analyzed by XPS.

After complexation with $\text{Cu}(\text{OAc})_2$ the transitions of the resulting metallopolymer, $P_{OS}[Cu]$, showed slight hypsochromic shifts in the UV range indicating ligand (polymer)-to-metal charge transfer effects (LMCT). It appears that the complexation caused significant quenching effects on the transitions

at 393 nm (D) and 470/504 nm (E) in the visible region (inset in Figure 2a). The broad and weak absorption band in the range of 600–700 nm is assigned to the d–d transitions of copper complexes [24], which is—compared to the $\text{Cu}(\text{OAc})_2$ —slightly shifted to lower wavelengths (Figure 2a, inset).

The chemical states of the polymer P_{OS} and its metallopolymer $\text{P}_{\text{OS}}[\text{Cu}]$ were analyzed by X-ray photoelectron spectroscopy (XPS). Figure 2b shows the binding energies (BE) of the 2p electrons of the copper centers in the polymer $\text{P}_{\text{OS}}[\text{Cu}]$. The binding energies of $\text{P}_{\text{OS}}[\text{Cu}]$ showed that the metallopolymer exhibited 22% of Cu(I) species with a remarkably high fraction of Cu(II) shake-up satellites (40%). The shake-up peaks in transition metals complexes are discussed as indicative charge-transfer effects between metal and ligands [25,26]. A similar polymer based on the same PHAM structure, the poly(isonaphthalene) methine reported by Sariciftci et al. [27] spontaneously reacts with molecular oxygen leading to post-oxidized polymers. Here, the post-oxidation of the polymer was possibly triggered by the redox chemistry of the copper, which remained as a reduced species in the polymer. Copper is known to be partly reduced by x-ray radiation under ambient conditions during the sample analysis [28] that can also be assisted by ligand effects. Nonetheless, the high content of Cu(I) follows the trend of the previously reported Cu metallopolymer with a redox-active moiety [22].

The O(1s) core level spectrum in the P_{OS} sample (Figure 3a) exhibited a broad sulfone ($\text{R}_1\text{R}_2\text{SO}_2$) fitting centered at 533.0 eV and strongly overlapping the phenol and other O-functional groups, which then became much less pronounced in the $\text{P}_{\text{OS}}[\text{Cu}]$ material (533.4 eV). In the latter sample, phenol/phenoxy O(1s) appeared as dominating functional groups in the fit envelope which were centered at 532.5 eV. The oxides centered at 531.7 eV and appearing as the second dominating fitting originated from oxygen attached to metals indicating complex formation ($\text{P}_{\text{OS}}[\text{M}]$, Figure 1).

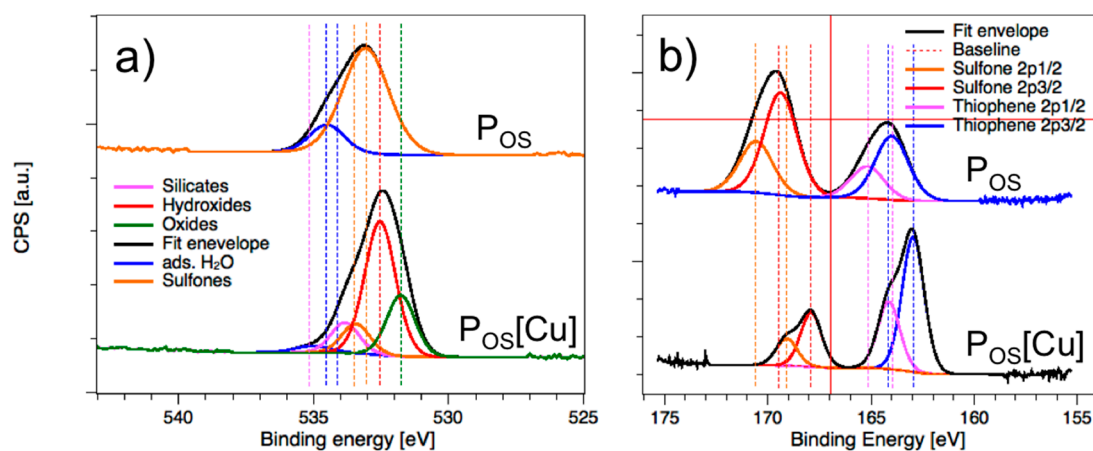


Figure 3. (a) O(1s) and (b) S(2p) core-level spectra of the analyzed samples P_{OS} (top) and $\text{P}_{\text{OS}}[\text{Cu}]$ (bottom) by X-ray photoelectron spectroscopy.

The S(2p) core-level spectra of the polymer P_{OS} and its metal hybrid $\text{P}_{\text{OS}}[\text{Cu}]$ exhibited two distinct binding energies with different ratios in intensity indicating mixtures of thiophene and sulfone functional groups (Figure 3b), each [22,29,30]. In both materials, the fitted binding energies appeared with the typical S(2p) doublet with 2/1 ratio and 1.2 eV splitting [30]. However, the most interesting feature of the S(2p) core level spectra is the change in the intensities from sulfone functional group being the major species in P_{OS} to the thiophene in $\text{P}_{\text{OS}}[\text{Cu}]$ and the significant shift to lower binding energies for both groups. The reduction of the sulfone content in S(2p) after complexation is consistent with the trend observed in the O(1s) core level data. After complexation with metal, the S(2p) doublets (S2p_{3/2} and S2p_{1/2}) appeared more distinctive in the envelope showing much narrower width of the fittings in total ($\text{P}_{\text{OS}}[\text{Cu}]$, Figure 3b).

In total, all atoms in $\text{P}_{\text{OS}}[\text{Cu}]$ involved in the coordination of the copper centers were at about 1–2 eV lower in their binding energies compared to those obtained from the pure polymer indicating

electronic impacts from the copper centers. The atomic ratio of 3.45/2.05 between sulfur and copper in $P_{OS}[Cu]$ survey spectrum (Figure S1, supporting information) is more indicative for a tridentate coordination mode (Figure 1) around the Cu centers. The tridentate mode becomes more clear if we consider 78% of the available copper in the oxidation +2, which then results in a S/Cu(II) ratio of 2.16/1.0 per repetition unit.

3.2. Photophysical Properties

The photocurrent measurements of the pure polymer P_{OS} and its metallopolymer $P_{OS}[Cu]$ were undertaken in a photoelectrochemical cell (PEC) using a platinum wire as a counter electrode (CE) and $Ag|AgCl$ (3 M KCl) as a reference electrode (RE). P_{OS} and $P_{OS}[Cu]$ deposited on a gold substrate acted as working electrodes (WE). For the deposition of the samples, we conducted two methods: The spin-coating technique and deposition via doctor blading method. The latter being a technique we already conducted for the deposition of inorganic metal oxides [31] in our previous work on photoelectrode fabrication. We found spin-coating to be the better option for this work due to the viscosity of the samples. Due to the varying solubility, different film thicknesses were obtained. The film thickness of $P_{OS}[Cu]$ was found to be 100 nm (± 10 nm) by ellipsometry methods, where the sample of the pure polymer could not be examined due to the higher thickness. Their photocurrent responses were recorded in a 0.1 M phosphate-buffered saline solution (PBS, pH 7.4) under dark conditions and illumination with 1.5 AM artificial solar light at their open circuit potentials.

Figure 4a shows the chronoamperograms of the polymer P_{OS} and its metallopolymer $P_{OS}[Cu]$ for the first 12 s under dark conditions and illumination with 1.5 AM artificial solar light (12 s). The current responses were recorded for 60 s under dark conditions and illumination for 12 s, each. The P_{OS} electrode showed a negative p-type response of $0.26 \mu A/cm^2$ (inset, Figure 4a) whereas the $P_{OS}[Cu]$ electrode showed an opposite n-type (4a) behavior of $2.6 \mu A/cm^2$ under the same conditions. The complexation of the conjugated polymer with copper turned the behavior of an intrinsically electron-accepting material (p-type) to an electron-donor (n-type). Although the thickness of the Cu(II)-doped film was much lower than the pure polymer film, the positive current density was, remarkably, 10 times higher than the current response of the pure polymer. Both electrodes respond with a sharp peak current (Figure 4a) that decays slowly during the turn on phase (photocurrent transients). The effect of photocurrent transient has been assigned to trapping of charges in the film and/or charge-accumulation at the semi-conductor-liquid junction [32–34].

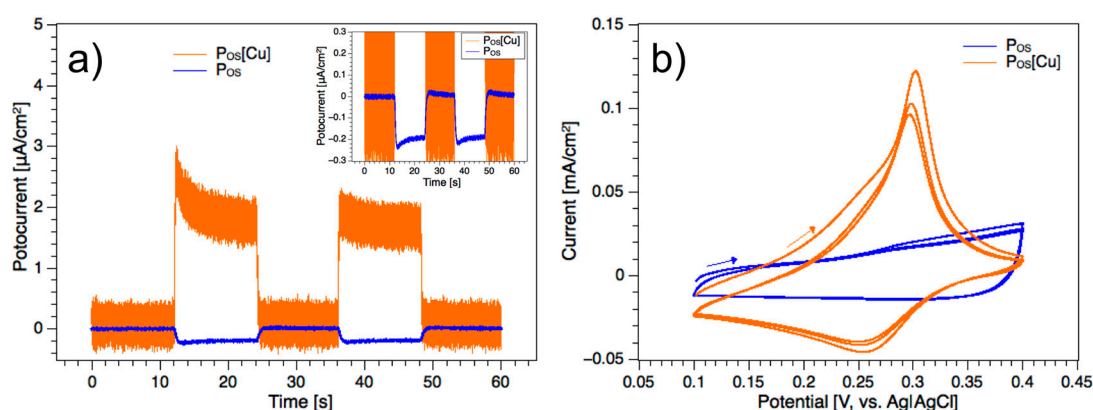


Figure 4. (a) Photocurrent response of the polymer and its copper complex in a 0.1 M saline solution; the photocurrents were recorded in the darkness for the first 12 s (s) followed by another 12 s under 1.5 AM artificial sunlight and again for 12 s darkness and 12 s light exposure, respectively; (b) cyclic voltammogram of both samples in 0.1 M KCl electrolyte solution in the potential range of 0.1–0.4 V and at a scan rate of 50 mV/s.

The electron donor behavior of $P_{OS}[Cu]$ and the results from XPS were corroborated by electrochemical investigations as it revealed copper centers in the oxidation state I. Figure 4b shows the cyclic voltammograms of P_{OS} and $P_{OS}[Cu]$ in a 0.1 M KCl solution. The copper complex shows a strong oxidation event at 0.29 volts vs. $Ag|AgCl$ (3 M KCl) which is assigned to the redox couple $Cu(I/II)$, whereas no redox peaks could be observed in the same potential range for the polymer. It is known that metal doping increases the photocurrent response of CPs [35,36]. However, to the best of our knowledge, the change of the photophysical behavior of CPs from p-type to n-type photoresponse in conjunction with metal complexation has not been reported yet.

3.3. Electrocatalytic Hydrogen Evolution Reaction (HER)

Earth abundant transition metals and their molecular structures are of great interest because of their potential to replace expensive platinum-group metals in the photo/-electrocatalytic water splitting [37–40]. The P_{OS} and $P_{OS}[Cu]$ electrodes were placed in an electrochemical cell and tested for the electrocatalytic hydrogen generation (HER). Here, P_{OS} and $P_{OS}[Cu]$ were drop casted on gold substrates and swept in 0.1 M PBS solution between 0.65 and -0.85 V vs. RHE. Their catalytic activities for HER were compared to a platinum disk electrode and a bare Au substrate. As shown in Figure 5a, the cyclic voltammograms of the gold and polymer electrodes are similar and the obtained peak current densities were at around -5 mA/cm^2 at -0.85 V, both. During the potentiometric sweeping, slight gas bubbles were observed at the polymer and gold electrodes at -0.85 V vs. RHE. Since the gold electrode [41,42] is known to act as a HER catalyst itself, the generated hydrogen at the polymer electrode is most likely caused by the gold under layer. Nonetheless, the copper metallopolymer electrode $P_{OS}[Cu]$ showed a much higher gas evolution rate at the working electrode. The hydrogen reduction was already initiated at a low overpotential of -300 mV vs. RHE (inset, Figure 5a) and exhibited a peak current density of -25 mA/cm^2 at -850 mV, which is five times higher than what was obtained at the metal free and gold electrodes (Figure 5a). The evolved H_2 was confirmed by GC analysis (Figure S2, supporting information). After 30 subsequent potentiometric sweeping, no polymer leaching or significant decreases in current density could be observed. Additionally, as shown in Figure 5b, a reversible redox event appeared between 100 and 400 mV vs. RHE, which was not observed at the pure polymer electrode. The reversible redox peak is assigned to the $Cu(I/II)$ species. Notably, the reversible redox event became more intensive and sharp with the increasing number of the potentiostatic sweeps indicating generation of more active redox species within the subsequent number of sweeps.

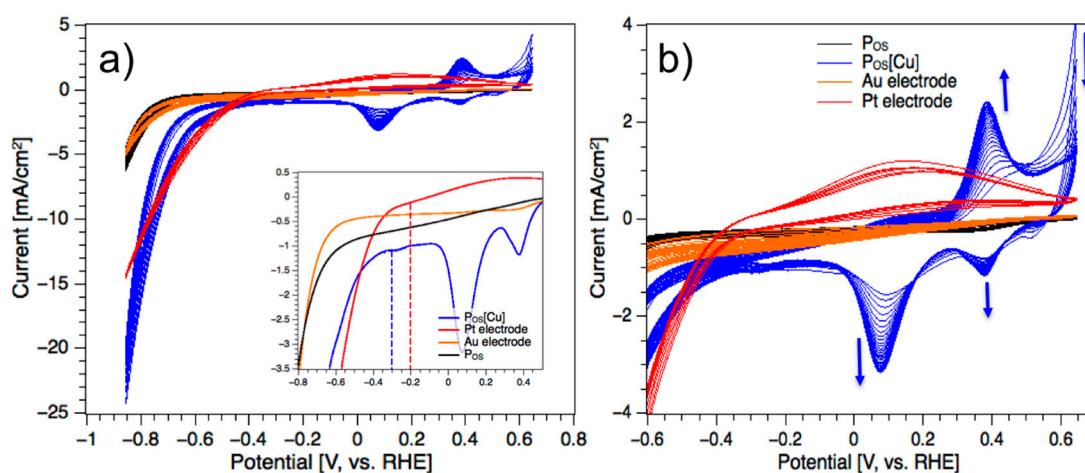


Figure 5. (a) Cyclic voltammogram of $P_{OS}[Cu]$ in 0.1 M PBS solution at a scan rate of 100 mV/s and 30 number of potentiometric sweeps compared to the polymer P_{OS} (16 sweeps), the Au substrate (18 sweeps) and the Pt electrode (7 sweeps); (b) cut-out of the CV from 5a highlighting the reversible redox peaks between 100 and 400 mV vs. RHE.

For comparison, a platinum disk was used under the same conditions. The hydrogen generation was initiated at -200 mV vs. RHE and the generated current density steadily increased up to 15 mA/cm² at the lower end potential. In the potential window between the onset reduction potential of -200 and -670 mV, it demonstrated higher performance than P_{OS}[Cu], but it was then overtaken by the metallopolymer catalyst at increased anodic overpotentials (Figure 5). The comparably lower peak current density at higher overpotentials is most likely caused by residing gas bubbles at the flat electrode surface causing a reduction of active surface area. This effect is overcome in the metallopolymer electrode because of the naturally porous structure of the hybrid catalyst and higher accessibility of the coordination sites for the water molecules.

At neutral pH, an efficient copper molybdenum sulfide electrocatalyst was reported to generate molecular hydrogen (H₂) at a reduction potential of -160 mV vs. RHE [43], which is 140 mV lower than the overpotential of the current P_{OS}[Cu] catalyst. The high activity of the reported Cu₂MoS₄ electrocatalyst, which mimics the active sites of the molybdenum CO-dehydrogenase, is associated with two possible intermediate states facilitating spontaneous H₂ evolution during the one-electron-reduction. However, the onset potential of P_{OS}[Cu] for the H₂ production is comparable to transition metal sulfide [44] and phosphide [45] catalysts, but is lower than the reduction potentials of protons obtained at, i.e., metal-free electrocatalysts [46], transition metals on carbon materials such as NiWS/CF [47] and Ni₂P/CNS [48], or molecular catalysts [49–51]. To obtain a current density of 10 mA/cm², the P_{OS}[Cu] and the blank Pt electrodes require an overpotential of 760 mV vs. RHE (Figure 5a) in neutral media, both. This overpotential is basically comparable to the efficient electrocatalysts Cu₂MoS₄ [43] and Ni-S [44] to obtain the same current density under same pH conditions.

4. Conclusions

To summarize, the combination of transition metals with conjugated/conducting polymers enables the exploration of hybrid organic/inorganic materials with manifold potential applications, which are yet to be explored. In the electrocatalytic hydrogen evolution reaction (HER), the copper-based metallopolymer reduced protons at a neutral pH and at overpotentials, which are only by 100 mV higher than the blank Pt electrode. To obtain a current density of 10 mA/cm² in the HER, the P_{OS}[Cu] catalyst requires overpotentials which are comparable to efficient platinum-free catalysts. The metallopolymer electrode showed stable performance after 30 sweeps without adding sacrificial agents and acidifying the electrolyte solution. The combination of a soft and easily processable conducting polymeric backbone with molecular catalyst enables the designing of new electrode materials made of well-defined single-site catalysts. The photophysical investigations of the P_{OS}[Cu] metallopolymer revealed a change of initially p-type photoresponse of the organic polymer to n-type behavior. The obtained current densities at the P_{OS}[Cu] photoelectrode were ten times higher than the metal-free one thus enabling new potentials in the design of photocatalysts.

Supplementary Materials: The following are available online at <http://www.mdpi.com/2073-4360/11/1/110/s1>, Figure S1: XPS survey spectrum of the polymer sample P_{OS}. Figure S2: XPS survey spectrum of the metallopolymer sample P_{OS}[Cu]. Figure S3: (a) Gas chromatogram of the reference gas (200 ppm H₂) and (b) gas chromatogram obtained from the head-space during the HER.

Author Contributions: Conceptualization, S.E.; Methodology, S.E.; Software, S.E.; Validation, S.E. and T.J.M.; Formal Analysis, S.E., W.S. and T.J.M.; Investigation, S.E. and T.J.M.; Resources, T.N. and M.A.; Data Curation, S.E. and W.S.; Writing-Original Draft Preparation, S.E.; Writing-Review & Editing, S.E. and T.J.M.; Visualization, S.E.; Supervision, T.N. and M.A.; Project Administration, T.N. and M.A.; Funding Acquisition, M.A.

Funding: This research was supported by the Australian Government through the Australian Research Council's Discovery Projects funding scheme (project DP160102356). T.J.M would like to acknowledge the Ramsay Memorial Trust for their financial assistance.

Acknowledgments: This work was performed in part at the South Australian node of the Australian National Fabrication Facility under the National Collaborative Research Infrastructure Strategy.

Conflicts of Interest: The authors declare no conflict of interest.

References

1. You, J.; Dou, L.; Yoshimura, K.; Kato, T.; Ohya, K.; Moriarty, T.; Emery, K.; Chen, C.-C.; Gao, J.; Li, G.; et al. A polymer tandem solar cell with 10.6% power conversion efficiency. *Nat. Commun.* **2013**, *4*, 1446. [[CrossRef](#)] [[PubMed](#)]
2. Xu, X.; Li, Z.; Wang, J.; Lin, B.; Ma, W.; Xia, Y.; Andersson, M.R.; Janssen, R.A.J.; Wang, E. High-performance all-polymer solar cells based on fluorinated naphthalene diimide acceptor polymers with fine-tuned crystallinity and enhanced dielectric constants. *Nano Energy* **2018**, *45*, 368–379. [[CrossRef](#)]
3. Bundgaard, E.; Krebs, F. Low band gap polymers for organic photovoltaics. *Sol. Energy Mater. Sol. Cells* **2007**, *91*, 954–985. [[CrossRef](#)]
4. Brabec, C.J.; Gowrisanker, S.; Halls, J.J.M.; Laird, D.; Jia, S.; Williams, S.P. Polymer-Fullerene Bulk-Heterojunction Solar Cells. *Adv. Mater.* **2010**, *22*, 3839–3856. [[CrossRef](#)]
5. Thompson, B.C.; Fréchet, J.M.J. Polymer–Fullerene Composite Solar Cells. *Angew. Chem. Int. Ed.* **2008**, *47*, 58–77. [[CrossRef](#)] [[PubMed](#)]
6. Forrest, S.R. The path to ubiquitous and low-cost organic electronic appliances on plastic. *Nature* **2004**, *428*, 911–918. [[CrossRef](#)] [[PubMed](#)]
7. Whittell, G.R.; Hager, M.D.; Schubert, U.S.; Manners, I. Functional soft materials from metallopolymers and metallosupramolecular polymers. *Nat. Mater.* **2011**, *10*, 176–188. [[CrossRef](#)]
8. Heinze, J.; Frontana-Urbe, B.A.; Ludwigs, S. Electrochemistry of Conducting Polymers—Persistent Models and New Concepts. *Chem. Rev.* **2010**, *110*, 4724–4771. [[CrossRef](#)]
9. Elmas, S.; Beelders, W.; Bradley, S.J.; Kroon, R.; Laifersky, G.; Andersson, M.; Nann, T. Platinum Terpyridine Metallopolymer Electrode as Cost-Effective Replacement for Bulk Platinum Catalysts in Oxygen Reduction Reaction and Hydrogen Evolution Reaction. *ACS Sustain. Chem. Eng.* **2017**, *5*, 10206–10214. [[CrossRef](#)]
10. Jenekhe, S.A. A class of narrow-band-gap semiconducting polymers. *Nature* **1986**, *322*, 345–347. [[CrossRef](#)]
11. Roncali, J. Molecular Engineering of the Band Gap of π -Conjugated Systems: Facing Technological Applications. *Macromol. Rapid Commun.* **2007**, *28*, 1761–1775. [[CrossRef](#)]
12. Bhushan, B.; Kumar, S.K.; Talwar, S.S.; Kundu, T.; Singh, B.P. Nonlinear optical properties of novel tunable, one dimensional molecular superlattice polymers (heteroarylene methines) containing alternating aromatic and quinoid segments. *Appl. Phys. B* **2012**, *109*, 201–209. [[CrossRef](#)]
13. Yi, W.; Feng, W.; Cao, M.; Wu, H. Synthesis of third-order non-linear optical polymers based on conjugated poly(heteroarylene methines). *Polym. Adv. Technol.* **2004**, *15*, 431–438. [[CrossRef](#)]
14. Wu, Z.; Wu, S.; Lu, Z.; Liang, Y. Organization and Properties of a Conjugated Poly(heteroarylene methines) at the Air–Water Interface and in the Langmuir–Blodgett Films. *J. Colloid Interface Sci.* **2002**, *251*, 125–130. [[CrossRef](#)] [[PubMed](#)]
15. Kato, A.; Fukushima, Y. Study of the Interaction between a Water-Soluble Cationic Poly(heteroarylene methine) and DNA. *J. Photopolym. Sci. Technol.* **2013**, *26*, 171–174. [[CrossRef](#)]
16. Gherras, H.; Hachemaoui, A.; Yahiaoui, A.; Benyoucef, A.; Belfedal, A.; Belbachir, M. Chemical synthesis and characterization of a new soluble conducting polymer. *Synth. Met.* **2012**, *162*, 1750–1755. [[CrossRef](#)]
17. Zhang, Q.; Li, Y.; Yang, M. A novel low band gap polymer PDTNTBQ. *Synth. Met.* **2004**, *146*, 69–71. [[CrossRef](#)]
18. Yang, M.; Zhang, Q.; Li, Y. A low band gap silicon-containing polymer. *J. Mater. Sci.* **2006**, *41*, 2533–2535. [[CrossRef](#)]
19. Chen, W.-C.; Jenekhe, S.A. Model compound studies of small bandgap conjugated poly(heteroarylene methines). *Macromol. Chem. Phys.* **1998**, *199*, 655–666. [[CrossRef](#)]
20. Zhang, Q.; Li, Y.; Yang, M. Novel soluble low band gap polymers. *J. Mater. Sci.* **2004**, *39*, 6089–6091. [[CrossRef](#)]
21. Yang, M.; Zhang, Q.; Wu, P.; Ye, H.; Liu, X. Influence of the introduction of phenylene units into the polymer backbone on bandgap of conjugated poly(heteroarylene methines). *Polymer* **2005**, *46*, 6266–6273. [[CrossRef](#)]
22. Elmas, S.; Beelders, W.; Pan, X.; Nann, T. Conducting Copper(I/II)-Metallopolymer for the Electrocatalytic Oxygen Reduction Reaction (ORR) with High Kinetic Current Density. *Polymers* **2018**, *10*, 1002. [[CrossRef](#)]
23. Chen, W.-C.; Jenekhe, S.A. Small-Bandgap Conducting Polymers Based on Conjugated Poly(heteroarylene methines). 1. Precursor Poly(heteroarylene methylenes). *Macromolecules* **1995**, *28*, 454–464. [[CrossRef](#)]

24. De M. Romanowski, S.M.; Tormena, F.; dos Santos, V.A.; de F. Hermann, M.; Mangrich, A.S. Solution studies of copper(II) complexes as a contribution to the study of the active site of galactose oxidase. *J. Braz. Chem. Soc.* **2004**, *15*, 897–903. [[CrossRef](#)]
25. Biesinger, M.C.; Payne, B.P.; Grosvenor, A.P.; Lau, L.W.M.; Gerson, A.R.; Smart, R.S.C. Resolving surface chemical states in XPS analysis of first row transition metals, oxides and hydroxides: Cr, Mn, Fe, Co and Ni. *Appl. Surf. Sci.* **2011**, *257*, 2717–2730. [[CrossRef](#)]
26. Biesinger, M.C.; Lau, L.W.M.; Gerson, A.R.; Smart, R.S.C. Resolving surface chemical states in XPS analysis of first row transition metals, oxides and hydroxides: Sc, Ti, V, Cu and Zn. *Appl. Surf. Sci.* **2010**, *257*, 887–898. [[CrossRef](#)]
27. Neugebauer, H.; Kvarnström, C.; Brabec, C.; Sariciftci, N.S.; Kiebooms, R.; Wudl, F.; Luzzati, S. Infrared spectroelectrochemical investigations on the doping of soluble poly(isothianaphthene methine) (PIM). *J. Chem. Phys.* **1999**, *110*, 12108–12115. [[CrossRef](#)]
28. Skinner, W.M.; Prestidge, C.A.; Smart, R.S.C. Irradiation Effects During XPS Studies of Cu(II) Activation of Zinc Sulphide. *Surf. Interface Anal.* **1996**, *24*, 620–626. [[CrossRef](#)]
29. Wavhal, D.S.; Fisher, E.R. Hydrophilic modification of polyethersulfone membranes by low temperature plasma-induced graft polymerization. *J. Membr. Sci.* **2002**, *209*, 255–269. [[CrossRef](#)]
30. Wang, H.; Cheng, F.; Li, M.; Peng, W.; Qu, J. Reactivity and Kinetics of Vinyl Sulfone-Functionalized Self-Assembled Monolayers for Bioactive Ligand Immobilization. *Langmuir* **2015**, *31*, 3413–3421. [[CrossRef](#)]
31. Macdonald, T.; Xu, J.; Elmas, S.; Mange, Y.; Skinner, W.; Xu, H.; Nann, T. NiO Nanofibers as a Candidate for a Nanophotocathode. *Nanomaterials* **2014**, *4*, 256–266. [[CrossRef](#)] [[PubMed](#)]
32. Le Formal, F.; Sivula, K.; Grätzel, M. The Transient Photocurrent and Photovoltage Behavior of a Hematite Photoanode under Working Conditions and the Influence of Surface Treatments. *J. Phys. Chem. C* **2012**, *116*, 26707–26720. [[CrossRef](#)]
33. McNeill, C.R.; Hwang, I.; Greenham, N.C. Photocurrent transients in all-polymer solar cells: Trapping and detrapping effects. *J. Appl. Phys.* **2009**, *106*, 024507. [[CrossRef](#)]
34. Li, Z.; McNeill, C.R. Transient photocurrent measurements of PCDTBT:PC₇₀ BM and PCPDTBT:PC₇₀ BM Solar Cells: Evidence for charge trapping in efficient polymer/fullerene blends. *J. Appl. Phys.* **2011**, *109*, 074513. [[CrossRef](#)]
35. Yu, S.C.; Hou, S.; Chan, W.K. Synthesis, Metal Complex Formation, and Electronic Properties of a Novel Conjugate Polymer with a Tridentate 2,6-Bis(benzimidazol-2-yl)pyridine Ligand. *Macromolecules* **1999**, *32*, 5251–5256. [[CrossRef](#)]
36. Elmas, S.; Beelders, W.; Nash, J.; Macdonald, T.J.; Jasieniak, M.; Griesser, H.J.; Nann, T. Photo-doping of plasma-deposited polyaniline (PAni). *RSC Adv.* **2016**, *6*, 70691–70699. [[CrossRef](#)]
37. Karunadasa, H.I.; Chang, C.J.; Long, J.R. A molecular molybdenum-oxo catalyst for generating hydrogen from water. *Nature* **2010**, *464*, 1329–1333. [[CrossRef](#)]
38. Zhang, P.; Wang, M.; Gloaguen, F.; Chen, L.; Quentel, F.; Sun, L. Electrocatalytic hydrogen evolution from neutral water by molecular cobalt tripyridine–diamine complexes. *Chem. Commun.* **2013**, *49*, 9455. [[CrossRef](#)]
39. Zhang, P.; Wang, M.; Yang, Y.; Yao, T.; Sun, L. A Molecular Copper Catalyst for Electrochemical Water Reduction with a Large Hydrogen-Generation Rate Constant in Aqueous Solution. *Angew. Chem. Int. Ed.* **2014**, *53*, 13803–13807. [[CrossRef](#)]
40. Cao, J.-P.; Fang, T.; Fu, L.-Z.; Zhou, L.-L.; Zhan, S.-Z. First mononuclear copper(II) electro-catalyst for catalyzing hydrogen evolution from acetic acid and water. *Int. J. Hydrog. Energy* **2014**, *39*, 13972–13978. [[CrossRef](#)]
41. Winther-Jensen, B.; Fraser, K.; Ong, C.; Forsyth, M.; MacFarlane, D.R. Conducting Polymer Composite Materials for Hydrogen Generation. *Adv. Mater.* **2010**, *22*, 1727–1730. [[CrossRef](#)] [[PubMed](#)]
42. Gu, C.; Norris, B.C.; Fan, F.-R.F.; Bielawski, C.W.; Bard, A.J. Is Base-Inhibited Vapor Phase Polymerized PEDOT an Electrocatalyst for the Hydrogen Evolution Reaction? Exploring Substrate Effects, Including Pt Contaminated Au. *ACS Catal.* **2012**, *2*, 746–750. [[CrossRef](#)]
43. Tran, P.D.; Nguyen, M.; Pramana, S.S.; Bhattacharjee, A.; Chiam, S.Y.; Fize, J.; Field, M.J.; Artero, V.; Wong, L.H.; Loo, J.; et al. Copper molybdenum sulfide: A new efficient electrocatalyst for hydrogen production from water. *Energy Environ. Sci.* **2012**, *5*, 8912–8916. [[CrossRef](#)]
44. Jiang, N.; Bogoev, L.; Popova, M.; Gul, S.; Yano, J.; Sun, Y. Electrodeposited nickel-sulfide films as competent hydrogen evolution catalysts in neutral water. *J. Mater. Chem. A* **2014**, *2*, 19407–19414. [[CrossRef](#)]

45. Yu, Y.; Peng, Z.; Asif, M.; Wang, H.; Wang, W.; Wu, Z.; Wang, Z.; Qiu, X.; Tan, H.; Liu, H. FeP Nanocrystals Embedded in N-Doped Carbon Nanosheets for Efficient Electrocatalytic Hydrogen Generation over a Broad pH Range. *ACS Sustain. Chem. Eng.* **2018**, *6*, 11587–11594. [[CrossRef](#)]
46. Qu, L.; Zhang, Z.; Zhang, H.; Zhang, H.; Dong, S. Transformation from graphitic C₃N₄ to nitrogen-boron-carbon ternary nanosheets as efficient metal-free bifunctional electrocatalyst for oxygen reduction reaction and hydrogen evolution reaction. *Appl. Surf. Sci.* **2018**, *448*, 618–627. [[CrossRef](#)]
47. Lu, S.-S.; Shang, X.; Zhang, L.-M.; Dong, B.; Gao, W.-K.; Dai, F.-N.; Liu, B.; Chai, Y.-M.; Liu, C.-G. Heterostructured binary Ni-W sulfides nanosheets as pH-universal electrocatalyst for hydrogen evolution. *Appl. Surf. Sci.* **2018**, *445*, 445–453. [[CrossRef](#)]
48. Li, Y.; Cai, P.; Ci, S.; Wen, Z. Strongly Coupled 3D Nanohybrids with Ni₂P/Carbon Nanosheets as pH-Universal Hydrogen Evolution Reaction Electrocatalysts. *ChemElectroChem* **2017**, *4*, 340–344. [[CrossRef](#)]
49. Amin, M.A.; Ibrahim, M.M.; Gobouri, A.A.; Mersal, G.A.M.; Mostafa, N.Y.; Altalhi, T.; Al-Juaid, S. A newly synthesized single crystal zinc complex as molecular electrocatalyst for efficient hydrogen generation from neutral aqueous solutions. *Int. J. Hydrog. Energy* **2017**, *42*, 25980–25995. [[CrossRef](#)]
50. Tang, L.-Z.; Lin, C.-N.; Zhan, S.-Z. Effect of ligand modification on hydrogen production catalyzed by iron(III) complexes supported by amine-bis(phenolate) ligands. *Polyhedron* **2016**, *110*, 247–253. [[CrossRef](#)]
51. Liu, S.; Xin, Z.-J.; Lei, Y.-J.; Yang, Y.; Yan, X.-Y.; Lu, Y.-B.; Li, C.-B.; Wang, H.-Y. Thin Copper-Based Film for Efficient Electrochemical Hydrogen Production from Neutral Aqueous Solutions. *ACS Sustain. Chem. Eng.* **2017**, *5*, 7496–7501. [[CrossRef](#)]



© 2019 by the authors. Licensee MDPI, Basel, Switzerland. This article is an open access article distributed under the terms and conditions of the Creative Commons Attribution (CC BY) license (<http://creativecommons.org/licenses/by/4.0/>).